



**The Influence of Various Zirconia Contents on Crystallite Sizes, Shrinkage, and Physical and Mechanical Properties of Hydroxyapatite-Based Nanobiocomposites**

Rasha A. Youness<sup>1</sup>, Mohammed A. Taha<sup>2</sup>, Medhat A. Ibrahim<sup>1\*</sup>



*1 Spectroscopy Department, National Research Centre, El Buhouth St., 12622 Dokki, Giza, Egypt.*

*2 Solid State Physics Department, National Research Centre, El Buhouth St., 12622 Dokki, Giza, Egypt.*

### Abstract

Carbonated hydroxyapatite (CHA)-based nanocomposite powders with different zirconia ( $ZrO_2$ ) contents, up to 8 wt.%, were prepared using high-energy ball mill. Phase composition of the resultant nanocomposites was investigated by X-ray diffraction (XRD) technique. Moreover, the crystal size, lattice strain and dislocation density were calculated. In order to measure shrinkage, physical and mechanical properties of these nanocomposites, their powders have been consolidated and sintered at 1000 °C. The results revealed that the gradual increase in  $ZrO_2$  contents caused increase in the lattice strain and dislocation density. On the opposite side, their crystal sizes decreased with increasing  $ZrO_2$  content. Moreover, the mechanical properties including microhardness, compressive strength, Young's modulus, elastic modulus, bulk modulus, shear modulus and Poisson's ratio of the sintered nanocomposites were greatly improved with increased  $ZrO_2$  contents until they reached 7 GPa, 165 MPa, 57 GPa, 70 GPa, 47.5 GPa, 22 GPa and 0.267, respectively for the sample containing the highest  $ZrO_2$  content. However, in spite of the great importance of  $ZrO_2$  contents on the mechanical properties, they caused noticeable increases in the porosity of the sintered samples. Additionally, increasing of  $ZrO_2$  contents, up to 8 wt.%, reduced the shrinkage percentages from 12.3% to 9.5%.

**Keywords:** Hydroxyapatite-based nanobiocomposites; Crystallite size; Shrinkage measurement; Physical properties; Mechanical properties.

### Introduction

During the last few decades, great efforts have been exerted to discover the ideal biomaterials used for treating bone fractures arising from various diseases including trauma, tumors, etc. To date, ideal biomaterials have not been discovered as they must possess immense and unmet properties like appropriate mechanical and physical properties, high bioactivity and biocompatibility, and having various shapes to be valid for different biomedical applications [1]. In this respect, the most promising strategy for overcoming this problem is to manufacture composite materials using the mechanical alloy method (MA) which is suggested to be an attractive way to produce these required composites [2,3]. Following this principle, abundant biocomposites have been prepared with comprehensive investigation of their different properties in many research articles [2,4-8]. Owing to its close similarity to the minerals present in the human bones, hydroxyapatite (HA) is one of the most attractive biomaterials that can be extensively used for dental and orthopaedic

applications [9]. For further improvement in its solubility as well as biological significance, carbonate ( $CO_3^{2-}$ ) groups can be incorporated into its crystal structure giving A-type or B-type CHA when partially substituting hydroxyl or phosphate groups, respectively. Noteworthy, nano-sized CHA powders exhibit outstanding characteristics compared to micron-sized ones [10,11]. Due to low mechanical properties of HA, its clinical applications are restricted to non-load-bearing sites [12,13]. Accordingly, adding a reinforcement phase to CHA is considered to play an important role in improving these poor mechanical properties [14-17].  $ZrO_2$  is a bio-inert ceramic that exhibits excellent thermal, mechanical and cosmetic properties. Interestingly, the latter property is gained through its close resemblance to the color of human teeth. Based on these amazing properties,  $ZrO_2$  has been utilized in dental applications for the first time in the 1990s [18]. Furthermore,  $ZrO_2$  also displays antibacterial effect since it is insoluble in water and thus reduces the bacterial adhesion. In addition, it exhibits high corrosion-resistance along with excellent

\*Corresponding author e-mail: [medahmed6@yahoo.com](mailto:medahmed6@yahoo.com)

Receive Date: 07 August 2020, Revise Date: 31 August 2020, Accept Date: 15 January 2021

DOI: 10.21608/EJCHEM.2021.38296.2787

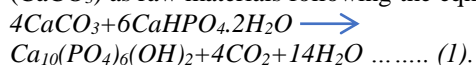
©2021 National Information and Documentation Center (NIDOC)

biocompatibility. In spite of these superior properties, its bio-inertness is the major drawback for expanding its clinical applications [3,12,19-21]. In this work, the effect of adding different weight percentages of ZrO<sub>2</sub> to CHA on shrinkage, and the physical and mechanical properties was investigated.

## Experimental procedure

### Preparation of CHA

Based on our recent articles [10,22], high-energy ball mill has been used to synthesize CHA nanopowders using calcium hydrogen phosphate dehydrate (CaHPO<sub>4</sub>.2H<sub>2</sub>O) and calcium carbonate (CaCO<sub>3</sub>) as raw materials following the eqn.:



### Preparation of CHA/ZrO<sub>2</sub> nanopowders

Pure ZrO<sub>2</sub> powders (99.99% purity; average particle size 200 nm), were purchased. Both ZrO<sub>2</sub> and CHA powders, based on their respective wt.%, were mechanically blended for 10 h with ball-to-powder ratio (BPR) equals to 2:1, speed 150 rpm and the diameters of balls were 10 mm. Then, planetary ball mill was utilized to perform the milling of these mixtures for 20 h with rotation speed equals to 450 rpm and BPR=15:1.

Table (1). The prepared samples with sample symbol and composition as a percentage.

Specimen code	Carbonated hydroxyapatite (CHA)	Zirconia (ZrO <sub>2</sub> )
Z0	100	0
Z2	98	2
Z4	96	4
Z8	92	8

### Phases evaluation of the prepared nanocomposites using XRD technique

The structure of the prepared CHA/ZrO<sub>2</sub> nanocomposites was examined by X-ray diffraction (XRD) technique, "Philips PW 1373" X-ray powder diffractometer with CuK-Ni filtered radiation. The crystallite size (D) and lattice strain ( $\varepsilon$ ) of the formed nanocomposites were calculated from the broadening (B) of two diffraction lines of CHA (1 1 2 and 3 0 0) according to the following eqns. mentioned in Refs. [23-25]:

$$D = \frac{0.9 \lambda}{B \cos \theta} \quad (2)$$

$$\varepsilon = \frac{B}{4 \tan \theta} \quad (3)$$

where:  $\lambda = 1.54059 \text{ \AA}$  (Cu-Ni radiation), B is the full width at half maximum (FWHM) and  $\theta$  is the angle in radians.

### Shrinkage measurements

As described in Ref. [26], the linear shrinkage of specimens after their sintering at 1000 °C was calculated according to the following equation:

$$S_l = \left( \frac{L_i - L_f}{L_i} \times 100\% \right) \quad (4)$$

Where  $S_l$ ,  $L_i$  and  $L_f$  are the total shrinkage, initial and final diameters of the samples before and after sintering, respectively. It is important to highlight that the precise calculation of average value and standard deviation were ensured by measuring five readings for each nanocomposite sample.

### Density and porosity measurements

As recently reported in our work [27], consolidation of the milled powders into pellets of 16 mm in diameter and 4 mm in length was done using hydraulic press at 50 MPa. Subsequently, both bulk density and apparent porosity were measured according to Archimedes' method (ASTM: B962-13).

### Mechanical properties

As described in our recent articles [28-30], Vickers microhardness was measured using Shimadzu-HMV (Japan) microhardness tester with 100 g load under ambient laboratory conditions with a constant indenter dwell time of 15 s. At least five indentations were measured per specimen for each data point. The indentation was made using a square-based pyramidal diamond with face angle 136° with measuring microscope and video monitor:

$$Hv = 1.854 \frac{P}{D^2} \quad (5)$$

Microhardness was calculated according to ASTM: B933-09 while, compressive strength was measured according to ASTM E9.

The ultrasonic wave velocities (longitudinal and shear) propagating in the samples were obtained at room temperature, using pulse-echo technique MATEC Model MBS8000 DSP (ultrasonic digital signal processing) system with 5 MHz resonating. The values of Lame's constants, i.e.  $\lambda$  and  $\mu$  were obtained from the longitudinal ( $V_L^2$ ) and shear ( $V_s^2$ ) ultrasonic velocities as follows:

$$\lambda = \rho(V_L^2 - 2V_s^2) \quad (6)$$

$$\mu = \rho V_s^2 \quad (7)$$

$$L = \lambda + 2\mu \quad (8)$$

$$G = \mu \quad (9)$$

$$E = \mu \frac{3\lambda + 2\mu}{\lambda + \mu} \quad (10)$$

$$B = \lambda + \frac{2}{3}\mu \quad (11)$$

$$v = \frac{\lambda}{2(\lambda + \mu)} \quad (12)$$

## Results and discussion

### Phases evaluation of the prepared nanocomposites using XRD technique

In this work, XRD technique was employed to examine the structure of the prepared nanocomposites as shown in Fig. 1. From this figure, it can be seen that the characteristic peaks of CHA appear clearly which can be identified according to (JCPDS No. 19-0272) in terms of line positions at  $2\theta=32.19, 33.43, 25.74$  and  $34.19^\circ$  which correspond to (1 1 2), (3 0 0), (0 0 2) and (2 1 0), respectively. On the opposite side, those of monoclinic  $\text{ZrO}_2$  are in a good agreement with JCPDS No. 86-1450 in terms of lines positions at  $2\theta=28.05, 31.47, 34.16$  and  $24.05^\circ$  which correspond to (1<sup>-</sup>1 1), (1 1 1), (0 0 2) and (0 1 1) reflections, respectively. As expected, the increased contents of  $\text{ZrO}_2$  are responsible for the observed increases in the peaks' intensities of  $\text{ZrO}_2$ , while those

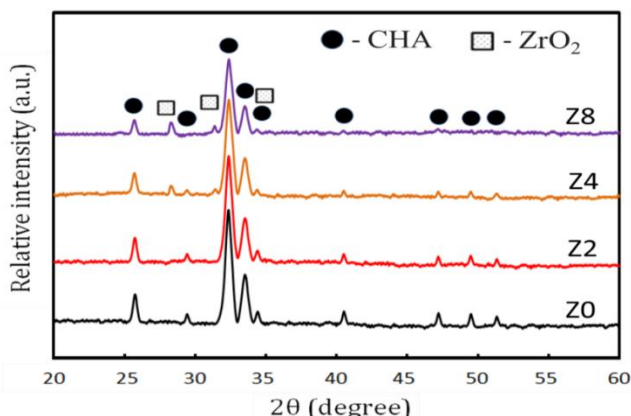


Fig. 1. XRD patterns of CHA-based nanocomposites powders with different  $\text{ZrO}_2$  contents (wt.%).

of CHA considerably decreased taking into account that the characteristic peaks of  $\text{ZrO}_2$  began to appear when its content increased to 4 wt.%. Importantly, the absence of other phases indicates that the prepared nanocomposites are contamination-free and the absence of a chemical reaction between CHA and  $\text{ZrO}_2$ .

Under the effect of adding different weight percentages of  $\text{ZrO}_2$ , CHA undergoes noticeable changes in its crystal size, lattice strain and dislocation density. Therefore, they were calculated using broadening analysis as shown in Figs. 2 and 3. On the basis of these figures, we can deduce that the successive increases in  $\text{ZrO}_2$  contents are responsible for the observed broadening in the characteristic peaks of CHA, causing considerable decreases in their crystals sizes. On the other hand, both dislocation density and lattice strain increased with increasing  $\text{ZrO}_2$  contents. These results can be better

explained by knowing that the existence of  $\text{ZrO}_2$  induces significant lattice distortion and refinement

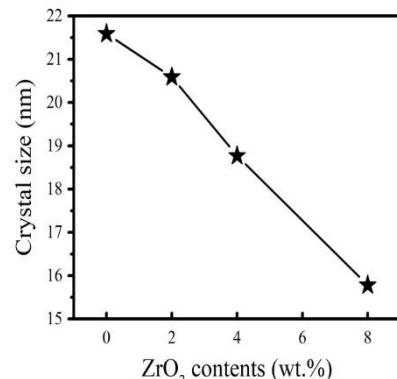


Fig. 2. Crystals sizes of CHA/ $\text{ZrO}_2$  nanocomposites powders versus  $\text{ZrO}_2$  contents (wt.%).

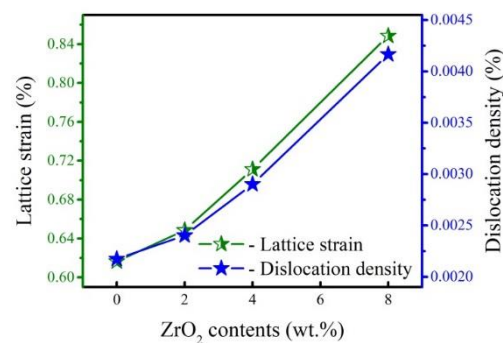


Fig. 3. Dislocation density and lattice strain of CHA/ $\text{ZrO}_2$  nanocomposites powders versus  $\text{ZrO}_2$  contents (wt.%).

of grains sizes leading to the noticed broadness with reduction in peaks' intensities [31]. The calculated crystal sizes of the prepared nanocomposites are 21.5, 20.5, 18.5 and 15.5 nm. However, lattice strain of these nanocomposites is 0.62, 0.65, 0.70 and 0.84%. The obtained results are consistent with those found in the literature [32-34].

### Shrinkage measurements

The shrinkage percentages for samples sintered at 1000 °C are illustrated in Fig. 4. It is possible to see that the shrinkage percentage decreased with increasing  $\text{ZrO}_2$  contents. The recorded percentages for Z0 and Z8 samples were 12.3 and 9.5%, respectively. The obtained results can be interpreted by considering the effectiveness of CHA nanoparticles to enhance the sinterability of the sintered samples and thus, the grains became strongly bound together. On the contrary, increasing the contents of  $\text{ZrO}_2$  is responsible for a considerable weakness in the sinterability where it requires higher temperature. These results are in a good agreement with the literature [3,26,35,36].

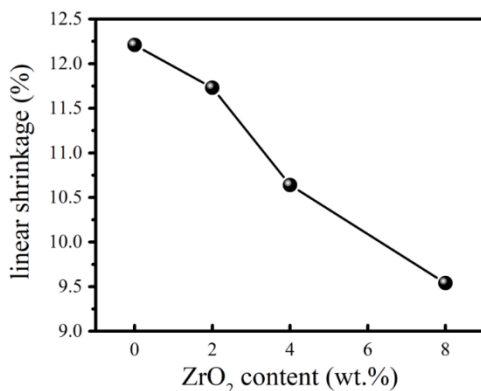


Fig. 4. Shrinkage percentages of the sintered nanocomposites samples.

### Density and porosity measurements

Generally, the dependence of density values of porosity contents and growth of crystalline particles are well-known [37]. In this regard, bulk density as well as apparent porosity of all sintered nanocomposites at 1000 °C were measured and illustrated in Fig. 5. It can be seen that bulk density increased by increasing ZrO<sub>2</sub> contents from 2.8 to 3.4 g/cm<sup>3</sup> for Z0 and Z8 specimens, respectively. The large difference between the bulk density of ZrO<sub>2</sub> (5.68 g/cm<sup>3</sup>) and HA (3.18 g/cm<sup>3</sup>) is the major reason for obtaining such result. Also, the porosity also increased by increasing ZrO<sub>2</sub> contents from 2.85 to 3.5% for Z0 and Z8 specimens, respectively. This result may be due to the large porosity of ZrO<sub>2</sub> compared to that of HA [38]. With the help of our recent article [10], low sintering temperature was chosen to avoid the possible CHA decomposition that results in the formation of other undesirable phases such as tricalcium/tetracalcium phosphate and calcium zirconate having in mind that these phases may negatively affect the different properties of the sintered samples [39].

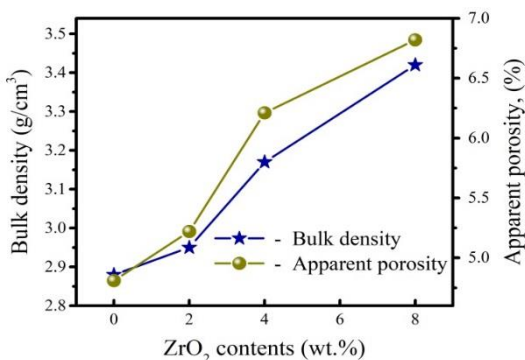
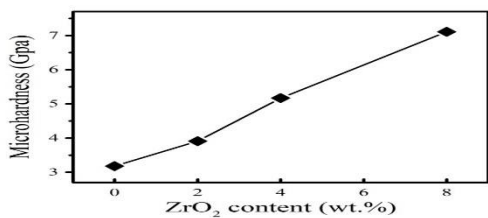
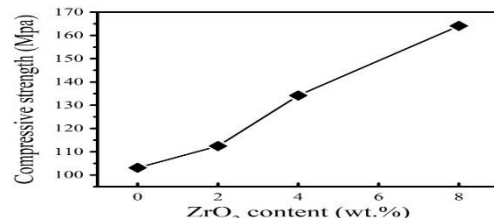
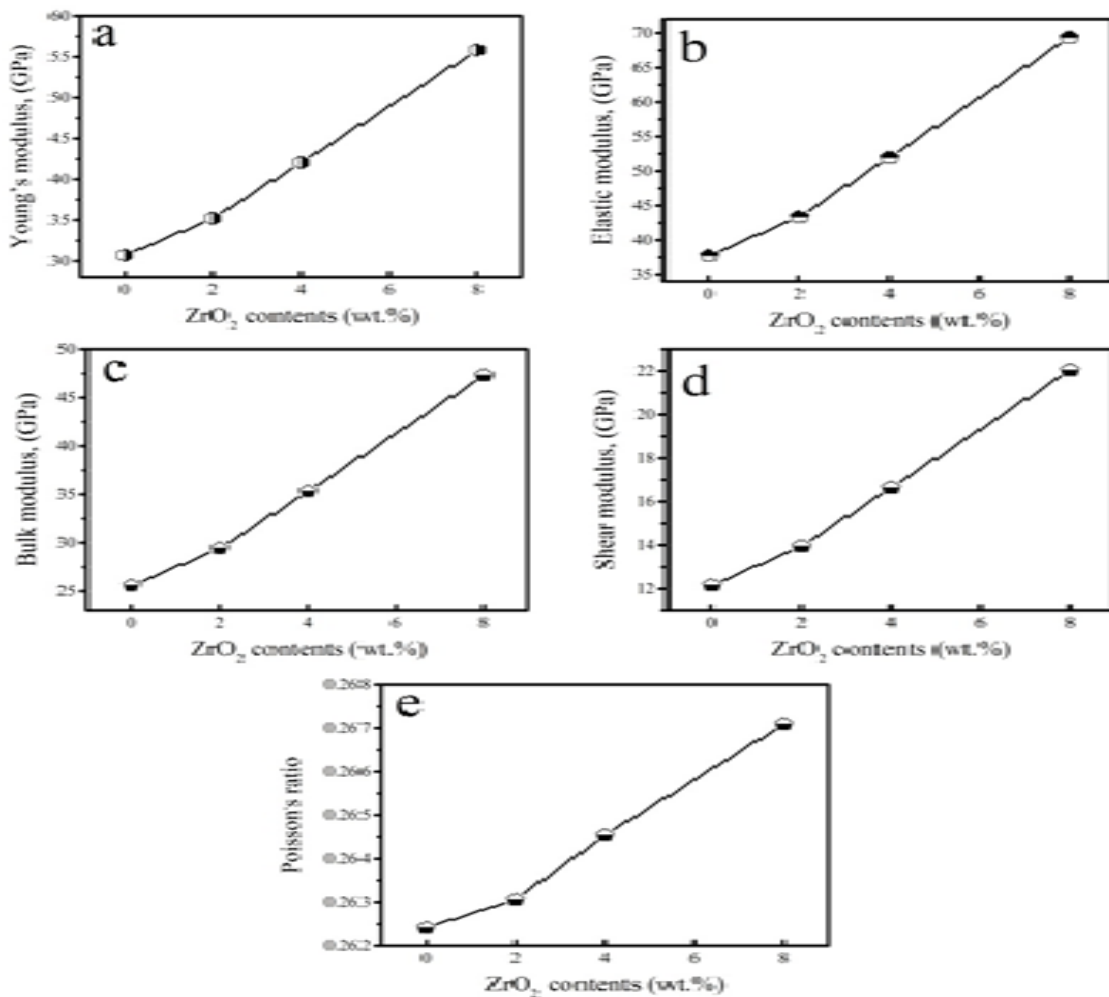


Fig. 5. Bulk density and apparent porosity of the sintered nanocomposites.

According to Ref. [40], obtaining good densification behavior for sintered samples is conditional upon choosing a suitable sintering temperature. Actually, sintering process occurs through different steps. At the beginning, the prepared powders should be compacted to facilitate the contact between the particles keeping in mind that firm bonding is not obtained. Later, when sintering temperature reaches 2/3 of the melting point, "necks" between particles are formed which give a firm bonding. Finally, the particles are no longer seen individually due to their complete bonding with each other. In addition, the mechanical properties of the sintered nanocomposites are not influenced by the porosity because of the closed pores. Interestingly, the presence of particles with high surface area consistent with high surface free energy is the driving force of this process. In contrast to the negative impact of porosity of sintered nanocomposites on their mechanical properties, it considerably improves their bioactivity behavior. This might be due to the ease of penetration of physiological fluids into the specimens which consequently, gives a better bioactivity manner. In accordance with these facts, an appropriate relationship is needed between the porosity and the mechanical properties of the material chosen for bone regeneration purposes [41].

### Mechanical properties

In general, obtaining appropriate mechanical properties for biomaterials is a great challenge. In this respect, microhardness (H<sub>v</sub>) and compressive strength are illustrated in Figs. 6 and 7, respectively, while the elastic moduli including Young's (Y), elastic (E), bulk (B) and shear (S) modulus along with Poisson's ratio (v) are represented in Fig. 8. From these figures, we can notice that the best mechanical properties were for Z8 specimen where ZrO<sub>2</sub> content is the highest. On the contrary, the worst were for Z0 sample. The recorded values of Z8 sample are 7 GPa, 165 MPa, 57 GPa, 70 GPa, 47.5 GPa, 22 GPa and 0.267, respectively. However, those of Z0 sample are 3 GPa, 100 MPa, 31 GPa, 37 GPa, 25 GPa, 12 GPa and 0.262, respectively. These results are in accordance with those reported in Section 3.1 and with the literature [42,43] which reported that the addition of high-strength materials like ZrO<sub>2</sub> is responsible for improving the mechanical properties of HA.

Fig. 6. Microhardness of the sintered CHA/ZrO<sub>2</sub> nanocompositesFig. 7. Compressive strength of the sintered CHA/ZrO<sub>2</sub> nanocomposites.Fig. 8. a) Young's (Y), b) elastic (E), c) bulk (B) and d) shear moduli and e) Poisson's ratio (v) of the sintered CHA/ZrO<sub>2</sub> nanocomposites.

### Conclusions

CHA/ZrO<sub>2</sub> nanocomposites powders with different ZrO<sub>2</sub> contents have been prepared by a high-energy ball mill. To measure physical and mechanical properties, these powders were consolidated and fired

at 1000 °C. The obtained results can be concluded in the following remarks:

- Increased ZrO<sub>2</sub> contents resulted in considerable decrease in the crystal size of the prepared nanocomposites. On the other hand, it was evident that lattice strain and dislocation density were obviously

- influenced by such increases in ZrO<sub>2</sub> weight percentages.
- Shrinkage values of nanocomposites were negatively affected by the decrease in CHA contents.
  - Bulk density of the sintered samples showed noticeable increase as ZrO<sub>2</sub> contents increased.
  - The apparent porosity of the samples increased with successive increases in ZrO<sub>2</sub> weight percentages.
  - Decreased CHA contents significantly enhanced all measured mechanical properties.
  - The obtained nanocomposites may be used in different clinical purposes.

### Conflicts of interest

There are no conflicts to declare.

### References

1. A. Bhowmick, N. Pramanik, P. Jana, T. Mitra, A. Gnanamani, M. Das, P.P. Kundu, *Int. J. Biol. Macromol.* 95 (2017) 348.
2. R.A. Youness, M.A. Taha, M.A. Ibrahim, *Mater. Chem. Phys.* 239 (2020): 122011.
3. T.A.I.C. Sartori, J.A. Ferreira, D. Osiro, L.A. Colnago, E.M.J.A. Pallone, *J. Eur. Ceram. Soc.* 38 (2018) 743.
4. R.A. Youness, M.A. Taha, M.A. Ibrahim, *J. Mol. Struct.* 1150 (2017) 188.
5. R.A. Youness, M.A. Taha, A.A. El-Kheshen, M. Ibrahim, *Ceram. Int.* 44 (2018) 20677.
6. R.A. Youness, M.A. Taha, M. Ibrahim, *Mater. Chem. Phys.* (2021) 123264.
7. M.A. Taha, R.A. Youness, M. Ibrahim, *Ceram. Int.* (2020) 23599.
8. A. Refaat, R.A. Youness, M.A. Taha, M. Ibrahim, *J. Mol. Struct.* 1147 (2017) 148.
9. A. Rezakhani, M.M.K. Motlagh, *Int. J. Phys. Sci.* 7 (20) (2012) 2768.
10. R.A. Youness, M.A. Taha, H. Elhaes, M. Ibrahim, *J. Comput. Theor. Nanosci.* 14 (2017) 2409.
11. M.E. Hassan, Jun Bai1, D.-Q. Dou, *Egypt. J. Chem.* 62 (9) (2019) 1725.
12. S. Priyadarsini, S. Mukherjee, M. Mishra, *J. Oral Biol. Craniofac. Res.* 8 (2018) 58.
13. C. Kailasanathan, N. Selvakumar, V. Naidu, *Ceram. Int.* 38 (2012) 571.
14. S. Vahabzadeh, M. Roy, A. Bandyopadhyay, S. Bose, *Acta Biomater.* 17 (2015) 47.
15. R.J. Kane, H.E. Weiss-Bilka, M.J. Meagher, Y. Liu, J.A. Gargac, G.L. Niebur, D.R. Wagner, R.K. Roeder, *Acta Biomater.* 17 (2015) 16.
16. H. Zhou, J. Lee, *Acta Biomater.* 7 (2011) 2769.
17. W. Que, K.A. Khor, J.L. Xu, L.G. Yu, *J. Eur. Ceram. Soc.* 28 (2008) 3083.
18. G.S. Kalayaraj, V. Vishwakarma, A.M.K. Kirubaharan, *Ceram. Int.* 44 (2018) 9780.
19. W. Kantana, P. Jarupoom, K. Pengpat, S. Eitssayeam, T. Tunkasiri, G. Rujiyanagul, *Ceram. Int.* 39 (2013) S379.
20. P. Bartolo, J.P. Kruth, J. Silva, G. Levy, A. Malshe, K. Rajurkar, M. Mitsuishi, J. Ciurana, M. Leu, *CIRP Ann.-Manuf. Technol.* 61 (2012): 635–655.
21. M.E.M. Ali, S.M. Abdel Moneim, H.S. Ibrahim, N.S. Ammar, H.K. El-Kholy, A.G. El-Deen, M.K. Zahran, M.H. Helal, *Egypt. J. Chem.* 63 (2) (2020) 515.
22. R.A. Youness, M.A. Taha, H. Elhaes, M. Ibrahim, *Mater. Chem. Phys.* 190 (2017) 209.
23. M.F. Zawrah, R.A. Essawy, H.A. Zayed, A.H. Hassan, M.A. Taha, *Ceram. Int.* 40 (2014) 31.
24. M.F. Zawrah, H.A. Zayed, R.A. Essawy, A.H. Hassan, M.A. Taha, *Mater. Des.* 46 (2013) 485.
25. R.M. Almoselhy, M.M. Eid, S.M.M. Abd-Elmageed, R.A. Youness, *Egypt. J. Chem.* 63 (7) (2020) 203.
26. L.F. Hu, C.A. Wang, *Ceram. Int.* 36 (2010) 1697.
27. R.A. Youness, M.A. Taha, M. Ibrahim, *Ceram. Int.* 44 (2018) 21323.
28. R.A. Youness, M.A. Taha, A.A. El-Kheshen, N. El-Faramawy, M. Ibrahim, *Mater. Res. Express* 6 (2019) 075212.
29. E.M.A. Khalil, R.A. Youness, M.S. Amer, M.A. Taha, *Ceram. Int.* 44 (7) (2018) 7867.
30. R.A. Youness, M.A. Taha, M. Ibrahim, A. El-Kheshen, *Silicon* 10 (2018) 1151.
31. M.A. Taha, M.F. Zawrah, *Ceram. Int.* 43(15) (2017) 12698.
32. E.B. Moustafa, M.A. Taha, *Appl. Phys. A* 126 (2020) 220.
33. M.F. Zawrah, H. Abo Mostafa, M.A. Taha, *Mater. Res. Express* 6 (2019) 125014.
34. M.A. Taha, G.M. Elkomy, H. Abo Mostafa, E. Gouda, *Mater. Chem. Phys.* 206 (2018) 116.
35. S. Farhangdoust, A. Zamanian, M. Yasaei, M. Khorami, *Mater. Sci. Eng. C* 33 (1) (2013) 453.
36. S. Deville, E. Saiz, A.P. Tomsia, *Biomaterials* 27 (32) (2006) 5480.
37. S. Laasri, M. Taha, E.K. Hlil, A. Laghzizil, A. Hajjaji, *C.R. Mecanique* 340 (2012) 715.
38. F. Bollino, E. Armenia, E. Traquillo, *Mater.* 10 (7) (2017) 757.
39. A.E. Hannora, S. Ataya, *Alloys Compd.* 658 (2016) 222.
40. M. Prakasam, J. Locs, K. Salma-Ancane, D. Loca, A. Largeateau, L. Berzina-Cimdina, *J. Funct. Biomater.* 6 (2015) 1099.
41. M.A. Encinas-Romero, J. Peralta-Haley, J.L. Valenzuela-Garcia, F.F. Castillon-Barrza, *Biomater. Nanotechnol.* 4 (2013) 327.
42. S.M. Naga, A.M. Hassan, M. Awaad, A. Killinger, R. Gadow, A. Bernstein, M. Sayed, *J. Asian Ceram. Soc.* 8 (2) (2020) 373.
43. C.H. Leong, A. Muchtar, C.Y. Tan, M. Razali, N.F. Amat, *Sintering of hydroxyapatite/yettria stabilized zirconia nanocomposites under nitrogen gas for dental materials*, *Adv. Mater. Sci. Eng.* 2014 (2014): 1-6.